Biomaterials Science

ROYAL SOCIETY OF CHEMISTRY

PAPER

View Article Online
View Journal | View Issue

Cite this: *Biomater. Sci.*, 2025, **13**, 1449

Construction of strontium-loaded injectable lubricating hydrogel and its role in promoting repair of cartilage defects†

Congcong Duan, ‡[a,c] Hongyue Jiang,‡[b] Shichen Zhang,[a,c] Yixing Wang,[a,c] Peng Liu,[a,c] Bin Xu,[b] Wenjing Tian *[b] and Bing Han *[a,c]

Received 22nd September 2024,
Accepted 15th November 2024

DOI: 10.1039/d4bm01260g

rsc.li/biomaterials-science

Injuries such as articular cartilage defects are prevalent factors in the development and progression of joint diseases. The discontinuity of the articular surface due to cartilage defects significantly accelerates the onset of arthritis. Cartilage tissue-engineered scaffolds are essential for restoring the continuity of the articular surface. This study presents a dual-network hydrogel, GelMA-FT/Sr^{2+}, which demonstrates excellent lubrication properties and accelerates the healing of cartilage defects. The hydrogel is composed of a methacrylated gelatin (GelMA) network, an *N*-fluorenylmethoxycarbonyl-L-tryptophan (FT) network, and strontium ions (Sr^{2+}). The results indicate that the hydrogel exhibits lubricating properties, and the incorporation of Sr^{2+} extends the degradation time of the hydrogel. Additionally, the hydrogel shows biocompatibility and enhances chondrogenic differentiation of bone marrow-derived mesenchymal stem cells (BMSCs) into cartilage. *In vivo* studies further confirm the hydrogel's efficacy in promoting the repair of cartilage defects in a rat model of cartilage injury. In conclusion, the GelMA-FT/Sr^{2+} hydrogel is a promising scaffold for cartilage tissue engineering, notable for its excellent lubrication properties, ability to recruit stem cells, and effectiveness in facilitating cartilage defect repair.

1. Introduction

Articular cartilage is a terminal tissue with no progenitor cells and lacks vascular and nerve supply, making self-repair challenging when damaged by high-impact sports, trauma, inflammation, tumors, or degenerative changes from aging or inactivity.[1] Articular cartilage covers the joints and provides one of the most effectively lubricated surfaces in nature.[2] This lubrication is crucial for joint health, and its disruption is associated with joint dysfunction, such as osteoarthritis (OA). OA often involves damage to the articular cartilage,[3] leading to a loss of lubrication. The increased friction on the cartilage surface causes progressive structural and functional damage, which exacerbates the inflammatory response and can result in joint failure, pain, and disability.[4] Current treatments are predominantly conservative, including fomentation, physical therapy, and intra-articular injections.[5] While these methods offer short-term relief, they are not sustainable in the long term.[6] As the disease progresses and organic lesions develop, more invasive procedures, such as arthroplasty, become necessary. Techniques for cartilage defect repair include bone marrow stimulation, granulated cartilage transplantation, autologous chondrocyte implantation (ACI), and cartilage grafting.[7] With advances in biomaterials science, tissue engineering is increasingly emerging as a key strategy for tissue defect repair.

Hydrogels are hydrophilic materials, which can be homopolymers, copolymers, or macromolecular monomers crosslinked to form a three-dimensional network with tunable physical properties and interconnected pore structures. These properties allow hydrogels to mimic the extracellular matrix environment, interact with cells, and mediate cell adhesion. Due to their similarity to cartilage tissue, hydrogels are at the forefront of research for treating cartilage defects.[8] Unlike preshaped scaffolds, which may not conform well to the defect morphology and can cause additional trauma due to the need for open implantation surgery, hydrogels are partially fluidic and can be injected to form a gel *in situ* at the defect site *in vivo*. Smart hydrogels, inspired by natural principles and structures, have found widespread application in artificial joints and tissues. Zhang *et al.* developed a shear-responsive supramolecular lubricating hydrogel for cartilage replacement

[a]*Department of Oral and Maxillofacial Surgery, School and Hospital of Stomatology, Jilin University, Changchun 130021, China. E-mail: hbing@jlu.edu.cn*
[b]*State Key Laboratory of Supramolecular Structure and Materials, Department of Chemistry, Jilin University, Changchun 130012, China. E-mail: wjtian@jlu.edu.cn*
[c]*Jilin Provincial key Laboratory of Tooth Development and Bone Remodeling, Changchun 130021, China*

†Electronic supplementary information (ESI) available. See DOI: https://doi.org/10.1039/d4bm01260g

‡These authors contributed equally to this article

by mimicking the dynamic lubrication mechanism of articular cartilage.[9] They synthesized this biomimetic hydrogel by combining a thixotropic supramolecular network with a polymeric bi-network. The shear-triggered disassembly of the *N*-fluorenylmethoxycarbonyl-L-tryptophan (FT) supramolecular network imparted a unique shear-responsive lubrication function to the hydrogel, which demonstrated gel-to-sol transition ability under shear force.[10]

The hydrogel can serve as a carrier for slow-release loading factors or drugs, acting locally on the lesion site. Doping specific ions into biomaterials is a well-documented advanced strategy for articular cartilage repair.[11] Strontium, a trace element, has been reported to positively impact cartilage and subchondral bone health.[12] In the early 1900s, it was observed that replacing a calcium diet with a strontium-enriched diet led to severe rickets in rats; however, this rickets caused by strontium ingestion could not be cured by vitamin D therapy.[13] Interestingly, the calcification capacity of the bones in these animals was reduced but not completely destroyed. Further studies demonstrated that strontium salts were deposited in hypertrophied cartilage *in vitro* when cartilage was immersed in a strontium solution.[14] It has been suggested that strontium significantly enhances the differentiation of adipose-derived stem cells (ADSCs) toward a chondrogenic lineage.[15] Yu Hao *et al.* examined the effects of strontium ranelate on the proliferation and chondrogenic differentiation of rat bone marrow-derived mesenchymal stem cells (BMSCs) *in vitro*. Their results indicated that strontium ranelate at 0.25 mM did not inhibit BMSCs proliferation and instead promoted chondrogenic differentiation.[16]

In this study, we incorporated strontium ions into GelMA and combined it with *N*-fluorenylmethoxycarbonyl-L-tryptophan, which was light-cured to form a dual-network hydrogel. We hypothesized that the FT supramolecular network would provide lubrication to the defect area under shear force, while the continuous release of strontium ions would contribute positively to defect repair. The construction of this dual-network hydrogel addresses the limitations of GelMA hydrogels alone and enhances the repair of articular cartilage defects.

2. Materials and methods

2.1 Materials

Gelatin (aladdin), methacrylic anhydride (aladdin), dialysis bag (USA viskase), Irgacure 2959 (aladdin), *N*-fluorenylmethoxycarbonyl-L-tryptophan (aladdin), strontium chloride (aladdin), PBS, deionized water, DMEM-High Glucose Medium (Hyclone), DMEM/F12 medium (Hyclone), Collagenase II (Biosharp), ITS Media Supplement (Beyotime), transforming growth factor (TGF)-β3 (Solarbio), Fetal bovine serum (Clark), a penicillin–streptomycin solution (NCM Biotech), Calcein/PI Cell Viability/Cytotoxicity Assay Kit (Beyotime), Phalloidin (Beyotime), PCR Assay Kits (Yeasen), BCA Protein Assay Kit (Beyotime), western blot related reagents (epizyme) (Fig. 1).

2.2 Fabrication of GelMA

First, 10 g of gelatin was added to 90 ml of PBS buffer solution and stirred at 50 °C to form a homogeneous solution to obtain a 10% (w/v) gelatin solution. Methacrylic anhydride was added to the gelatin solution at 0.5 ml min^{-1} and stirred at 50 °C for 3 h. The reaction was terminated by dilution to 5 times the volume with PBS buffer solution. The resulting solution was dialyzed for 5 days at 40 °C using dialysis bags with a mole-

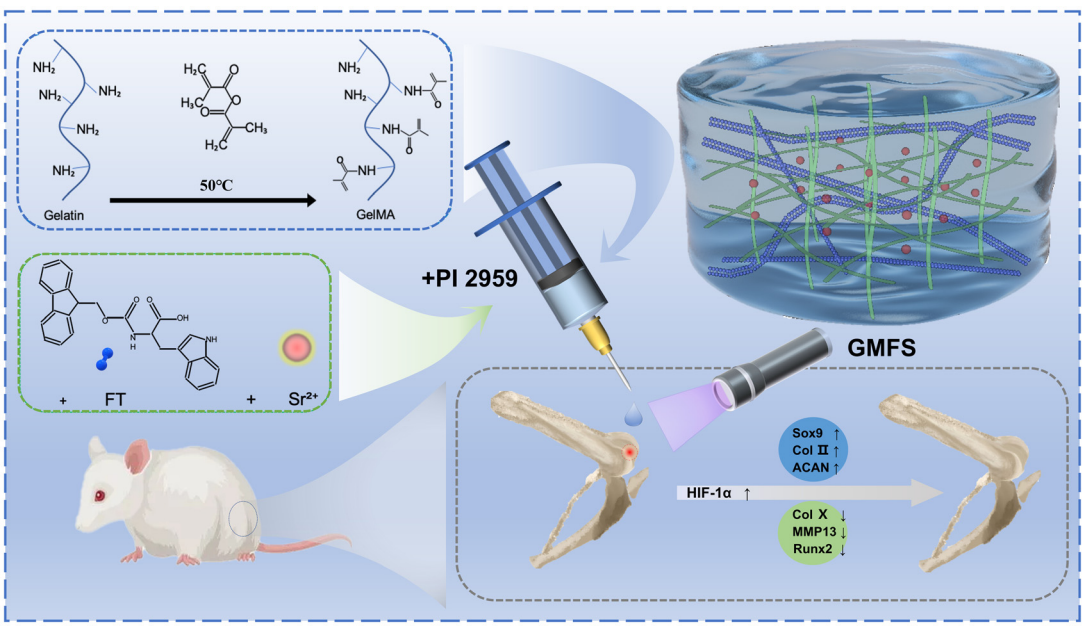

Fig. 1 Schematic illustration of the whole study.

cular weight cut-off of 3500 Da. After overnight in a refrigerator at −80 °C, it was placed in a lyophilizer for 48 h. The resulting sample was stored at −20 °C protected from light for spare use.

0.006 g of gelatin and GelMA were added to 0.6 mL of deuterated water (D_2O) respectively. After confirming that all the samples were fully dissolved and mixed homogeneously, the solutions were injected into clean NMR tubes. The tubes were placed into a 500 MHz NMR spectrometer for proton detection. The obtained data were analyzed using MestReNova software.

2.3 Preparation of hydrogels

The same weight GelMA samples were weighed, the first set was dissolved in deionized water at 50 °C and stirred to obtain a 10% (w/v) GelMA solution; the second set was dissolved in deionized water at 50 °C and stirred to obtain a 10% (w/v) GelMA solution and then strontium chloride was added to give a final concentration of 30 mM of Sr^{2+}; the third set was dissolved in deionized water at 50 °C and stirred to obtain a 20% (w/v) of GelMA solution, then an equal volume of prepared *N*-Fmoc-L-tryptophan (FT) solution (2 mg ml^{-1}) was added, and continued to stir well; the fourth group was dissolved in deionized water at 50 °C and stirred to obtain a 20% (w/v) of GelMA solution, an equal volume of prepared FT solution was added, and continued to stir well, and then strontium chloride was added to give a final concentration of 30 mM of Sr^{2+}. The Irgacure 2959 was added to all four solutions at a final concentration of 0.5% under light-avoiding conditions. The four groups of solutions were injected into a cylindrical PTFE mold, and the hydrogel was cured after 5 min of irradiation with a 365 nm UV light source. The four groups are labeled as GM, GMS, GMF and GMFS, respectively.

The FT monomer powder as well as the dehydrated solid pellets of the synthetic hydrogel were ground into powder in an onyx mortar at room temperature and tested on a Fourier infrared spectrometer using the KBr solid powder compact method in the frequency range of 4000 to 400 cm^{-1}, and the functional groups contained were determined by comparing and analyzing the peak positions of the specific absorption peaks of the materials.

2.4 Morphology of hydrogels

For morphological characterization, freshly prepared four groups hydrogels were frozen, lyophilized and subjected to SEM examination using a S-4800 field emission scanning electron microscope (Hitachi, Japan). The SEM images were taken at a voltage of 3 kV and a current of 10 μA. The current of gold injection was set to 10 mA and the time of gold injection was 90 s.

2.5 Mechanical properties

The hydrogel was made into a cylinder with a diameter of 12 mm and a height of 10 mm, placed on the lower pressure plate of the universal testing machine, and the cutting experiment was carried out with a cutter with a cutter thickness of 2 mm, so the initial contact area between the cutter and the hydrogel could be approximated as a rectangular area with a length of 12 mm and a width of 2 mm. A sensor with a load range of 0 to 2 kN was used to control the cutter movement in the vertical direction, and the loading rate was set to 10 mm min^{-1} by the sensor. The real-time changes of load and displacement during the movement were obtained, and the stress–strain curves of the hydrogel samples were plotted, which were repeated three times for each experimental group.

2.6 Degradation in aqueous media

Freshly prepared hydrogels of each group, weighed the initial weight of each group of samples, which was recorded as Wd, and added the hydrogel samples into Ep tubes, added PBS buffer according to the ratio of 0.2 g ml^{-1}, and put into the incubator at 37 °C. The degradation solution was changed every 3 days, and the hydrogel samples were taken out at certain time intervals (7 days, 14 days, 21 days, 28 days), the water on the surface of the hydrogel was gently absorbed with filter paper, and the weights of the hydrogel at different degradation times were weighed and recorded as W_t. This was repeated three times for each group. The weight retention rate of the hydrogel was obtained based on the initial weight of the hydrogel in each group, W_d, and the weight of the sample at the corresponding time point, W_t, and was calculated by the following formula:

$$\text{Sample weight retention rate } (\%) = (W_t/W_d) \times 100\%$$

2.7 Measurement of the swelling ratio

To detect the dynamic swelling behavior, the freshly prepared gels were weighed on a microbalance to record their initial wet weight (W_i), and the hydrogel samples were placed into a six-well plate with PBS buffer, submerged the hydrogel samples, and placed into a 37 °C incubator. The hydrogel samples were taken out at certain intervals (1 day, 3 days, 5 days, 7 days), and the water on the surface of the hydrogel was gently absorbed with filter paper, and the weight of the hydrogel at different immersion times was weighed and recorded as W_t until there was no significant change in the weight of the hydrogel. Each group was repeated three times. The swelling ratio of the hydrogels was obtained from the initial weight of the hydrogels in each group, W_i, and the swelling weight of the hydrogels at the corresponding time point, W_t, and the formula was as follows:

$$SR = (W_t/W_i) \times 100\%$$

2.8 Rheological tests

TA rotational rheometer was used to measure the rheological properties of the prepared hydrogels. Parallel plate grips and pal plates were used in the test, with an upper clamp diameter of 8 mm and a sample gap of 1 mm. The change of G' (storage modulus) and G'' (loss modulus) of the hydrogel with shear stress was measured in oscillation mode at room temperature, the angular frequency was set to 1 rad s^{-1} and the strain was

1%, evaluating the change in G' (storage modulus) and G'' (loss modulus) of hydrogels over time. The test was repeated three times for each experimental group.

2.9 Tribological tests

The friction of the hydrogels were measured using a DHR-2 rheometer (TA Instruments, USA). A fixture with a diameter of 8 mm was selected for measurement, and the shear velocity of 0.1 mm s^{-1} was fixed to explore the friction.

2.10 Cytocompatibility assay

2.10.1 Isolation and culture of rat bone marrow mesenchymal stem cells. The whole bone marrow apposition method was used to isolate BMSCs from SD rats. 2 Week-old male SD rats were taken and sterilized all over the body by soaking in 75% alcohol for 10 min, and the femur and tibia were separated under aseptic conditions in an ultra-clean bench, preserving the muscle on the surface of the bone, and then transferred to pre-cooled PBS, washed twice, the muscle on the surface of the bone was separated, and the cartilage on the femur and tibia was clipped off, and the marrow cavity was rinsed three times into a 100 mm dish using a 5 mL A syringe was used to aspirate complete medium (α-MEM medium + 10% FBS + 1% penicillin–streptomycin) to rinse the bone marrow cavity 3 times into a 100 mm Petri dish, and the bone marrow of one femur and one tibia was put into one Petri dish. Then the dishes were cultured in a 37 °C, 5% CO_2 cell culture incubator, with the first fluid change at day 3 and every 2 days thereafter, and the cells were passaged when they were full grown to about 90%, and the morphology of the cells was observed using an inverted phase contrast microscope.

2.10.2 Cell proliferation assay. The proliferative effects of hydrogels on BMSCs *in vitro* were detected using the Cell Counting Kit-8 (CCK-8). The extracts of four groups of hydrogels, GM, GMS, GMF and GMFS, were prepared according to ISO 10993.5. Briefly, *i.e.*, complete medium containing 10% FBS was used to incubate each group of hydrogels at 0.2 g mL^{-1} for 24 h at 37 °C, and the hydrogel extracts were prepared. Cells were inoculated in 96-well plates at an initial density of 2×10^3 cells per well, with 5 replicates per group, and the medium or extract was changed after 24 h of incubation in each group. The cells were changed every other day, and 110 μL of culture medium containing 10 μL of CCK-8 solution was added to each well after 1, 3 and 5 days of incubation, and the OD450 value was measured by an enzyme marker after 2 h of incubation.

2.10.3 Cell growth activity assay *in vitro*. The effect of each group of hydrogels on the growth activity of BMSCs was examined using a live-dead cell staining kit. The hydrogels in each group were gelatinized in a disc-shaped 12-well plate, and 2×10^4 cells were seeded per well, with 3 replicates in each group. The solution was changed every other day, and after 5 and 10 days, the live and dead cells were stained separately using a live and dead cell staining kit. A confocal laser scanning microscope was used to observe and take pictures.

2.10.4 Cell adhesion. To observe the cell adhesion on the hydrogels, BMSCs are seeded on hydrogel disks (1×10^4 cells per well) and cultured for 7 and 14 days. After immobilized by 4% paraformaldehyde for 20 minutes at room temperature, cells were permeabilized in 0.4% Triton X-100 solution for 10 minutes at room temperature. After washed in PBS, these disks were incubated in diluted 1 : 100 fluorescently labeled phalloidin solution for 20 minutes at room temperature, and counterstained in DAPI for 5 minutes. BMSCs morphology was observed with confocal laser scanning microscopy (CLSM).

2.11 Real-time PCR assay

RT-qPCR was used to detect the effects of hydrogels on the expression of genes related to chondrogenic differentiation of rat BMSCs, including *Sox9*, *Collagen type II* (*Col II*), *Aggrecan* (*Acan*), *Collagen type x* (*Col X*), matrix metallopeptidase 13 (*Mmp13*), and *Runx2*. Six-well plates were used, and each well was injected with 1 ml of each group of hydrogel and cured with UV light, rinsed with PBS, inoculated with 2×10^5 chondrocytes, and then replaced with chondrogenic induction medium when the cells were about 90% full grown. After that, the medium was changed every other day, and after 14 and 21 days of culture, respectively, the cells were digested using trypsin and collected. The total RNA of BMSCs was extracted using the Trizol method. The concentration and purity of the extracted RNA were detected using a Nano Drop 2000 Spectrophotometer. Following the steps in the instructions of the reverse transcription kit, the RNA was reverse transcribed to obtain cDNA, and the RT-qPCR reaction was performed using SYBR Green Master Mix. The relative expression of the above genes was calculated by using the 2-ΔΔCt method with the *GAPDH* gene of BMSCs as the internal reference gene. The primer sequences used in this experiment are shown in Table 1.

2.12 Western blot assay

Protein expression analysis was conducted after 14 and 21 days of culture, based on the protocols provided in section 2.11. Then a routine procedure was conducted for western blot. The expression of chondrogenic-related proteins: SOX9 (ET1611-56, Huabio, China), ACAN (DF7561, Affinity Biosciences, USA), and HIF-1α (CY5824, Abways, China) were tested, with β-actin used for normalization.

2.13 *In vivo* chondrogenesis studies

2.13.1 Animals. The experiment used 30 male SD rats of 12 week-old size, with a weight size of about 300 g. All the animal procedures were performed in accordance with the Guidelines for Care and Use of Laboratory Animals of Jilin University and approved by the Animal Ethics Committee of Jilin University (SYXK(Ji)2023-0010). All knees were equally divided into five groups: blank control group, GM group, GMS group, GMF group, and GMFS group. Under aseptic environment, a longitudinal incision of about 1.5 cm was made along the medial side of the patella, and the skin and subcutaneous tissues were incised to the joint capsule, then the patella was dislo-

Table 1 Primers used for qRT-PCR Chondrogenesis-related genes

Gene	Forward primer sequences	Reverse primer sequences
GAPDH	GGTCGGTGTGAACGGATTTGG	GCCGTGGGTAGAGTCATACTGGAAC
Sox9	GGCGGAGGAAGTCGGTGAAG	AGATGGCGTTAGGAGAGATGTGAG
Col II	ACGCTCAAGTCGCTGAACAAC	AATCCAGTAGTCTCCGCTCTTCC
Acan	CACAGGCAGCACAGACACTTC	GGAGTCAAGGTCGCCAGAGG
Col X	GGATGCCTCTTGTCAGTGCTAAC	GTCATAGTGCTGCTGCCTGTTG
Mmp13	ACAGTTGATAGACTCCGAGAAATGC	CACATCAGGCACTCCACATCTTG
Runx2	TCGTCAGCGTCCTATCAGTTCC	CTTCCATCAGCGTCAACACCATC

cated to the lateral side, revealing the talocalcaneal groove at the distal end of the femur. A defect with a diameter of 2 mm and a depth of 1.5 mm was prepared at the talar groove with a split drill. Except for the blank control group, the hydrogel solutions prepared in advance were injected into the defect, and the hydrogel was cured *in situ* by irradiation with a 365 nm ultraviolet light source for 5 min. The patella was repositioned, the joint cavity was closed, and the incision was closed in layers. Penicillin solution was injected intramuscularly daily for 3 days postoperatively to prevent infection. The rats were anesthetized and executed at 8 and 12 weeks postoperatively, and the material was taken and fixed with 4% paraformaldehyde. The experimental sites were photographed to observe and compare the effect of defect repair in each group.

2.13.2 Histological analysis and immunohistochemistry. The tissues were fixed with 4% paraformaldehyde for 24 h, then decalcified with 10% EDTA, gradient alcohol dehydration and embedded in sections, and then stained with HE staining, safranin O-solid green staining and immunohistochemical staining respectively.

2.14 Statistical analysis

Statistical analyses were performed using IBM SPSS Statistics 25.0 software for Windows. Data were presented as means ± standard deviation. The difference in the values between the two groups was determined by *t* test. The statistical significance of more than two groups was assessed using one-way ANOVA. A value of $*p < 0.05$ was considered statistical differences and $**p < 0.01$ and $***p < 0.001$ were considered statistically significant differences.

3. Results and discussion

3.1 Synthesis of hydrogels

Methacryloyl gelatin (GelMA) was first synthesized by Bulcke *et al.*[17] During the synthesis of GelMA, the amino groups on the side chains of gelatin were modified with methacrylic anhydride (MA) to introduce double bonds. To verify the successful synthesis of methacrylated gelatin, we conducted proton nuclear magnetic resonance (^{1}H NMR) spectroscopy on the synthesized product, as shown in Fig. 2a. The ^{1}H NMR spectrum of GelMA revealed new peaks compared to gelatin, with two peaks in the 5 to 6 ppm region indicating the presence of double-bonded protons ($=CH_2$) from methacrylic anhydride. Additionally, the GelMA spectrum showed reduced intensity of peaks between 2.5 and 3 ppm, suggesting a decrease in methylene ($-CH_2-$) groups due to the modification of lysine residues in gelatin. GelMA derivatives are highly susceptible to photoinduced reactions because of the high density of unsaturated photocrosslinking groups. Polymerization of GelMA in an aqueous environment occurs *via* a free radical mechanism in the presence of a photoinitiator. UV irradiation of the photoinitiator generates free radicals, which initiate chain growth polymerization. Photopolymerization offers several advantages, including injectability, rapid gelation, enhanced mechanical properties, suitability for custom bioprinting, and ease of incorporation into various cell types. The high density of methacryloyl groups has been reported to provide a protective effect on encapsulated cells.[18,19] GelMA also contains the arginine-glycyl-aspartate (RGD) tripeptide, which promotes cellular activities such as attachment, spreading, and differentiation, supports enzymatic degradation, and plays a crucial role in dermal wound healing, morphogenesis, and tissue repair.

The incorporation of functional groups in the hydrogels was assessed using fourier-transform infrared (FTIR) spectroscopy, with results presented in Fig. 2b. The spectra of the GM, GMS, GMF, and GMFS groups exhibited similar features. In the GMF and GMFS groups, a new peak at 748 cm^{-1} was observed, corresponding to the benzene ring in the FT hydrogels. In contrast, the GMS and GMFS groups, which contained strontium ions, showed a diminished O–H bending vibration peak at 858 cm^{-1}. This reduction is likely due to the coordination of Sr^{2+} with hydroxyl groups within or between the GelMA chains.

3.2 Morphology of hydrogels

After uniformly mixing the components according to the preparation method for each hydrogel group, as depicted in Fig. 2d, the hydrogels initially appeared as solutions. Upon UV irradiation for 5 minutes, the hydrogels solidified. When the sample bottles were tilted, the hydrogels remained settled at the bottom. To examine the microscopic network structure of the hydrogels, we labeled the four hydrogel groups as GM, GMS, GMF, and GMFS. After freeze-drying, the samples were rapidly quenched with liquid nitrogen and their morphology and structure were observed using a scanning electron microscope. As shown in Fig. 2c, the porosity of each hydrogel group ranged from 60–70%. The incorporation of FT increased the porosity, whereas the addition of Sr^{2+} reduced it, though the

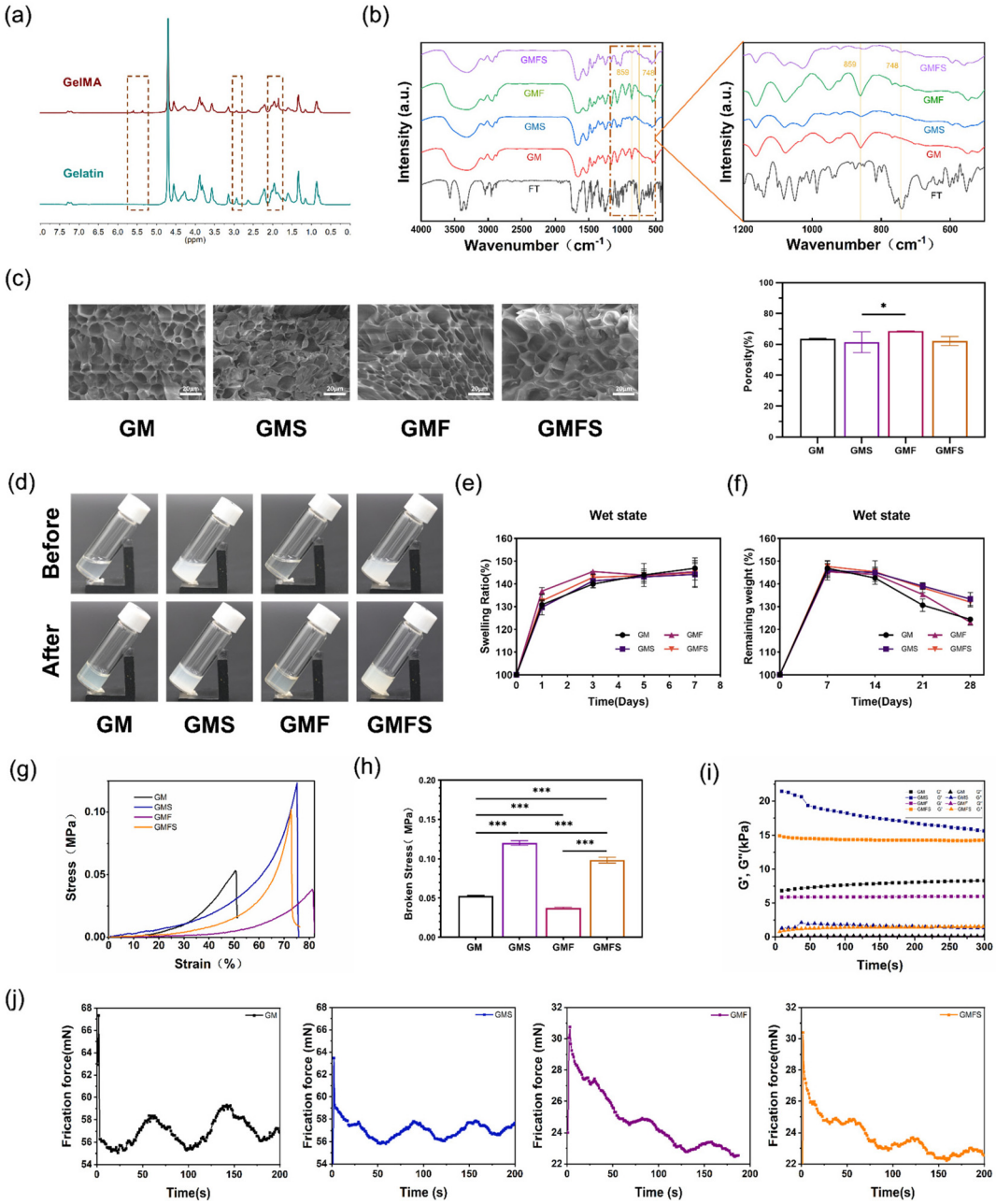

Fig. 2 Characterizations of the different hydrogel groups. (a) ^{1}H NMR spectra of gelatin and GelMA samples in D_2O. (b) FTIR spectra of FT, GM, GMS, GMF, GMFS. (c) SEM images and the average porosity of different hydrogels. (d) Liquid state of each group of hydrogels before UV irradiation and cured state after UV irradiation. (e) The swelling ratio of the samples at wet state (n = 3). (f) The remaining weight of the hydrogels at phosphate buffered saline (PBS) solutions (n = 3). (g) The compressive stress–strain curves and (h) tensile strength at break of the samples calculated from mechanical testing (n = 6) of the hydrogels. (i) Rheological test. (j) The variation of friction with time on the surface during the reciprocating friction motion (***p < 0.001, **p < 0.01, *p < 0.05).

difference was not significant. This observation, combined with the FTIR results, suggests that the coordination of Sr^{2+} with hydroxyl groups within or between GelMA chains may have led to tighter cross-linking of the GelMA network. The synergistic effect of intermolecular benzene ring π–π interactions and hydrogen bonding causes FT to self-assemble into a chain structure. Consequently, the introduction of new segments that intersect within the covalent network of the GelMA system may loosen the original network structure, potentially increasing its porosity.

3.3 The swelling ratio

The swelling ratios of the four hydrogel groups—GM, GMS, GMF, and GMFS—were determined using a weighing method.

As shown in Fig. 2e, the swelling of each hydrogel group gradually reached equilibrium after 3 days of immersion, with the swelling ratio stabilizing at 145 ± 6.5% after 7 days. The differences in swelling ratios among the four hydrogel groups were not statistically significant, indicating that the incorporation of FT and Sr^{2+} does not substantially affect the swelling properties of GelMA hydrogels. All four hydrogel groups demonstrated excellent water absorption capabilities, suggesting their potential for absorbing excess fluid in swollen joints to alleviate pain.[20]

3.4 Degradation in aqueous media

To investigate the fundamental degradation properties of hydrogels, we conducted *in vitro* weighing experiments to assess hydrogel degradation. We measured the wet weight of the hydrogels at various time points and calculated the weight retention rate of the samples. The results are illustrated in Fig. 2f. Our findings indicate that the weights of the four hydrogel groups remained relatively stable with no significant differences observed between the groups over 1–2 weeks. Additionally, the wet weights of the hydrogels were still above 120% of their initial weights after 4 weeks. The incorporation of the FT supramolecular hydrogel did not significantly affect the degradation of the GelMA cross-linking network. Conversely, the Sr^{2+}-containing GMS and GMFS hydrogels exhibited slower degradation compared to the GM and GMF hydrogels, with this difference being statistically significant ($P < 0.001$). Ideally, hydrogel degradation should align with the tissue regeneration rate at the defect site.[21] Excessive degradation can lead to underutilization of the scaffold's biological function. Furthermore, rapid degradation often results in insufficient mechanical strength. In our study, the presence of Sr^{2+} in the hydrogel delayed the degradation of GelMA, potentially providing extended support for the regenerative repair of cartilage.

3.5 Mechanical properties

As demonstrated in Fig. 2g and h, the incorporation of Sr^{2+} into the hydrogel network significantly enhanced its mechanical strength. We hypothesize that Sr^{2+} may form coordination bonds with the organic network of the hydrogel. In comparison, the mechanical strengths of the hydrogels in the GM and GMS groups were 0.05 ± 0.001 MPa and 0.12 ± 0.003 MPa, respectively. After introducing the FT supramolecular hydrogels, the mechanical strengths in both groups decreased. This reduction may be attributed to the interpenetration of the supramolecular FT chain segment with the polymer network, resulting in a looser network structure in the GMF and GMFS groups compared to the GM and GMS groups. Additionally, the FT supramolecular network is more susceptible to damage from external forces, leading to a decrease in overall hydrogel strength. Despite the reduction in mechanical strength with the addition of FT, the fracture strength of the GMFS group hydrogel remained above 0.1 MPa, indicating that it still possesses good mechanical properties. For bionic lubricating hydrogel materials, robust mechanical strength is essential. Gan *et al.* developed a shellfish-inspired strategy to enhance the mechanical properties of GelMA hydrogels by incorporating dopamine methacrylic acid (ODMA) oligomers into the GelMA chains.[22] This modification increased the toughness and elasticity of the hydrogel, which subsequently promoted the adhesion and growth of mesenchymal stem cells *in vitro* and supported cartilage regeneration *in vivo* when loaded with chondroitin sulfate or TGF-β3.

3.6 Lubrication and rheological properties

The expression of mechanosensitive genes in chondrocytes within cartilage tissue, including genes encoding cartilage-degrading enzymes, is regulated by biomechanical signals transmitted through friction-induced shear stress on cartilage surfaces. Consequently, investigating the impact of lubricants on this biomechanical signaling through *in vivo* experiments would be valuable.[3] Han Ying *et al.* developed an injectable hydrogel microsphere with enhanced lubrication and controlled drug release for osteoarthritis treatment. This was achieved by dip-coating the surface of GelMA microspheres with a self-adhesive polymer.[23] Dual functionality was attained by encapsulating the anti-inflammatory drug diclofenac sodium (DS) within the microspheres. The hydrogel microspheres demonstrated favorable therapeutic effects in a rat knee osteoarthritis model. Additionally, studies on friction in articular surfaces suggest that cartilage lubrication could be simulated in articular prostheses by creating self-lubricating surfaces that replicate the boundary layer of cartilage. Similarly, incorporating self-lubricating surfaces in tissue-engineered scaffolds for cartilage lesions may mitigate the effects of high-stress environments on these scaffolds.

Considering that the FT supramolecular network exhibits a gel–sol transition under shear force, we combined it with the GelMA polymeric network to explore its potential lubricating effect during this transition. The rheological behaviors of the four hydrogel groups were assessed over time, as illustrated in Fig. 2i. For all GelMA-based hydrogels, the storage modulus (G') exceeded the loss modulus (G''), indicating successful gelation. Additionally, the hydrogel group containing Sr^{2+} demonstrated higher storage and loss moduli compared to the group without Sr^{2+}. However, the inclusion of FT resulted in a reduction in the storage modulus. Despite this, the storage modulus of the hydrogel group containing both Sr^{2+} and FT remained significantly higher than that of the pure GelMA group. Friction experiments were conducted on each hydrogel group using a DHR-2 rheometer, and the friction variation over time during reciprocating motion was recorded, as shown in Fig. 2j. Under a fixed load and shear rate, the surface friction of each hydrogel group decreased following an initial peak. Comparative analysis revealed that the addition of FT significantly reduced surface friction, showing a continuous decrease over time. In contrast, hydrogels without FT exhibited cyclical fluctuations in surface friction after an initial reduction, rather than a continuous decline. The addition of Sr^{2+} did not significantly affect surface friction. This may be due to the shear force during friction causing the thixotropic FT supramolecular network near the surface to disassemble, converting the gel-state FT network into

monomers and fragments in the sol state. These fragments were pressurized and exuded to the hydrogel surface, forming a lubricating film between the hydrogel and the contact ball, thereby enhancing lubrication during reciprocal friction. With increasing shear cycles, the disassembly of FT supramolecular chain segments on the surface becomes more thorough, resulting in a continuous decrease in friction force.

3.7 Cytocompatibility assay

To evaluate the *in vitro* biocompatibility of GMFS hydrogels, we employed rat bone marrow mesenchymal stem cells (rBMSCs). The cells were cultured with either a standard complete medium or extracts from each hydrogel group (GM, GMS, GMF, and GMFS). Cell proliferation was assessed using the Cell Counting Kit-8 (CCK-8). In the early stages of the experiment, we prepared hydrogels with concentrations of 20 mM, 30 mM, and 40 mM of Sr^{2+}. We conducted cell proliferation experiments using hydrogels that contained no Sr^{2+} as well as those with varying concentrations of Sr^{2+}. The experimental results indicated that the GMFS hydrogels containing 30 mM Sr^{2+} effectively promoted cell proliferation (as shown in Fig. S1†). Therefore, in the subsequent experiments, we utilized both the GMS group and the GMFS group with a Sr^{2+} concentration of 30 mM. As illustrated in Fig. 3a, compared to the control group, cell proliferation increased after 1 and 3 days in cultures with extracts from all hydrogel groups. However, no significant differences were observed among the hydrogel groups. On day 5, the GMS and GMFS groups demonstrated enhanced cell proliferation relative to the other groups. Additionally, live/dead assays of rBMSCs revealed the presence of dead cells (red) in all groups after 7 and 14 days of culture (Fig. 3c). The corresponding quantitative statistical results for dead cells (Fig. 3b) indicated that, in the short term, the addition of Sr^{2+} or FT could reduce the proportion of dead cells; however, the difference was not statistically significant at 14 days. These findings indicate that the addition of supramolecular FT did not significantly affect cytotoxicity, while the inclusion of Sr^{2+} appeared to promote cell proliferation. Previous studies on arthritis treatments have shown that strontium inhibits chondrocyte apoptosis, thereby preventing cartilage destruction in arthritis.[24]

After 5 and 10 days of culture, the nuclei and actin cytoskeletons of the BMSCs were labeled with DAPI and phalloidin,

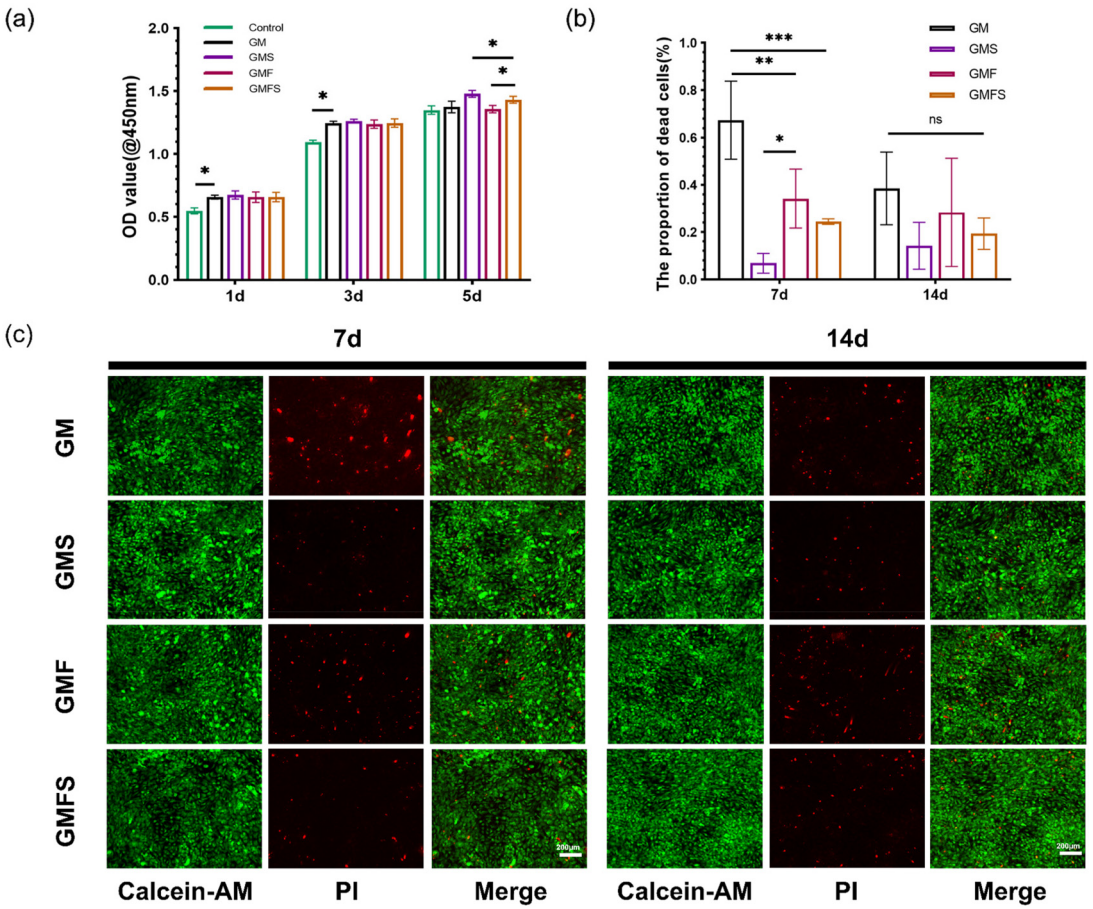

Fig. 3 Biocompatibility of various hydrogels. (a) OD values of BMSCs cultured for 1, 3, 5 days with normal complete medium and extracts from each group of hydrogels. (b) Quantitative data of dead cells and (c) the live/dead straining of BMSCs cultured on GM, GMS, GMF and GMFS for 7 and 14 days (*$p < 0.05$).

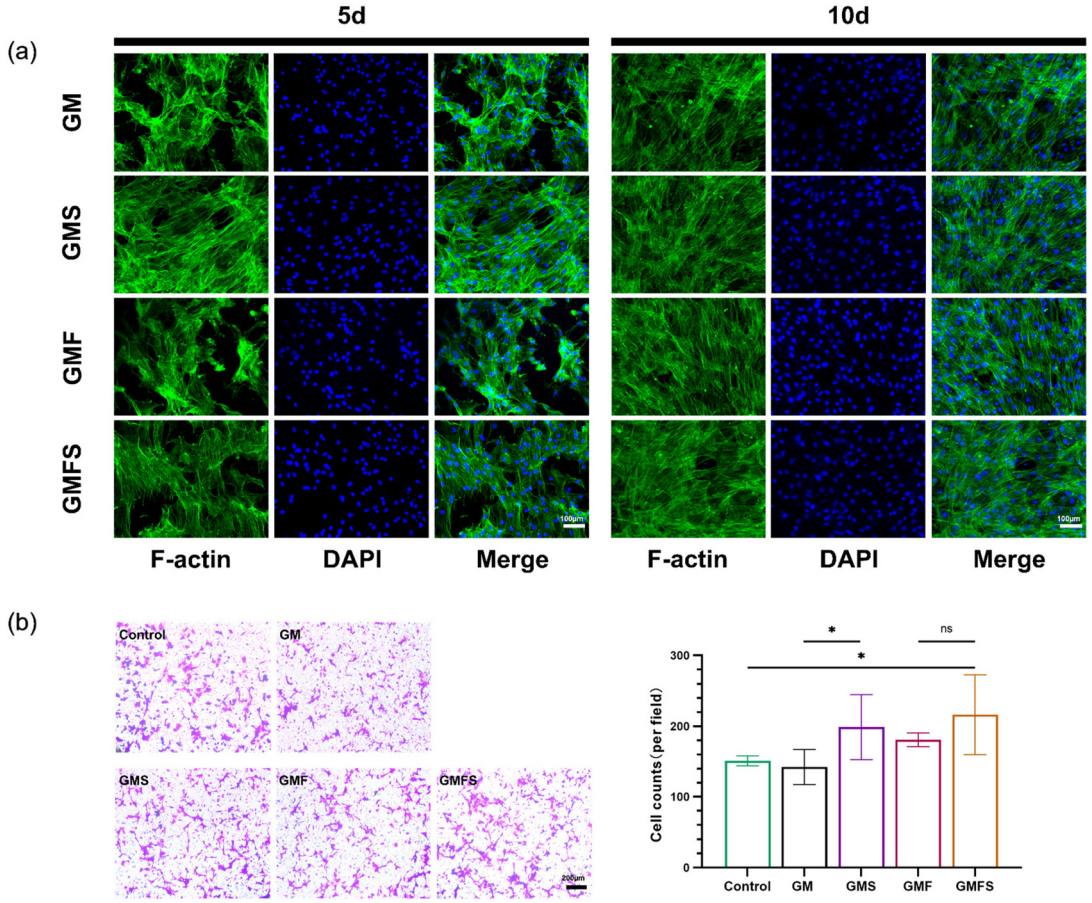

Fig. 4 (a) Phalloidin and DAPI staining of BMSCs cultured on GM, GMS, GMF and GMFS for 5 and 10 days. (b) Effects of different hydrogels on the migration of BMSCs *in vitro* (purple shows the cells) (*$p < 0.05$).

and their morphologies on the samples were observed using a confocal microscope. As shown in Fig. 4a, the cells appeared stretched into polygonal shapes on the hydrogel surface. At 5 days, the extent of diffusion and stretching of BMSCs in the GMS and GMFS groups was significantly greater compared to the GM and GMF groups, indicating that the addition of Sr^{2+} enhanced cell adhesion to the hydrogel.

To assess the impact of each hydrogel group on the ability of rat BMSCs to recruit and migrate, we conducted 48 hour migration experiments using Transwell chambers. The results, presented in Fig. 4b, were quantified after imaging under a microscope. The GMS and GMFS groups exhibited higher cell counts compared to the other groups ($p < 0.05$). Previous studies have reported that ionic dissolution products of calcium silicate-based materials containing strontium and titanium nanotubes, supported by Sr/Ag, can promote the migration of MC3T3-E1 cells.[25,26] To eliminate potential confounding factors, Zhou *et al.* incorporated strontium into micro/nano-rough titanium surfaces and verified the recruitment of Sr^{2+} on bone marrow mesenchymal stem cells both *in vitro* and *in vivo*. The mechanism may be related to the enhanced expression of the SDF-1α/CXCR4 signaling pathway induced by Sr^{2+}.[27] However, when Huang *et al.* investigated the effect of strontium on dental pulp stem cells, they found that the concentration of Sr that promoted cell proliferation did not enhance the migration of human dental pulp stem cells (hDPSCs).[28] The inconsistencies in results may be attributed to variations in strontium content, release kinetics, and cell species.

3.8 Effect of Hydrogels on the differentiation of BMSCs to cartilage *in vitro*

A previous study investigated the effects of exposing ADSCs to culture medium (CM) with or without Sr^{2+} (0.15–15.00 mM) for up to 14 days. CM containing 1.50 mM Sr^{2+} significantly enhanced the secretion of glycosaminoglycans (GAGs) and the mRNA expression of *Sox9* and *Col II-α1* compared to CM alone and basal medium.[15] In our study, we assessed the impact of each hydrogel group on the chondrogenic differentiation of BMSCs. After 14 and 21 days of co-culture with the hydrogels, we evaluated the expression of chondrocyte-related genes using RT-qPCR. The genes examined included *Sox9*, *Col II*, *Acan*, *Col X*, *Mmp13*, and *Runx2*. The results, shown in Fig. 5a–f, indicate that compared to the GelMA group, the addition of Sr^{2+} significantly promoted the expression of *Sox9*, *Col II*, and *Acan*, while suppressing *Col X*, *Mmp13*, and *Runx2* expression.

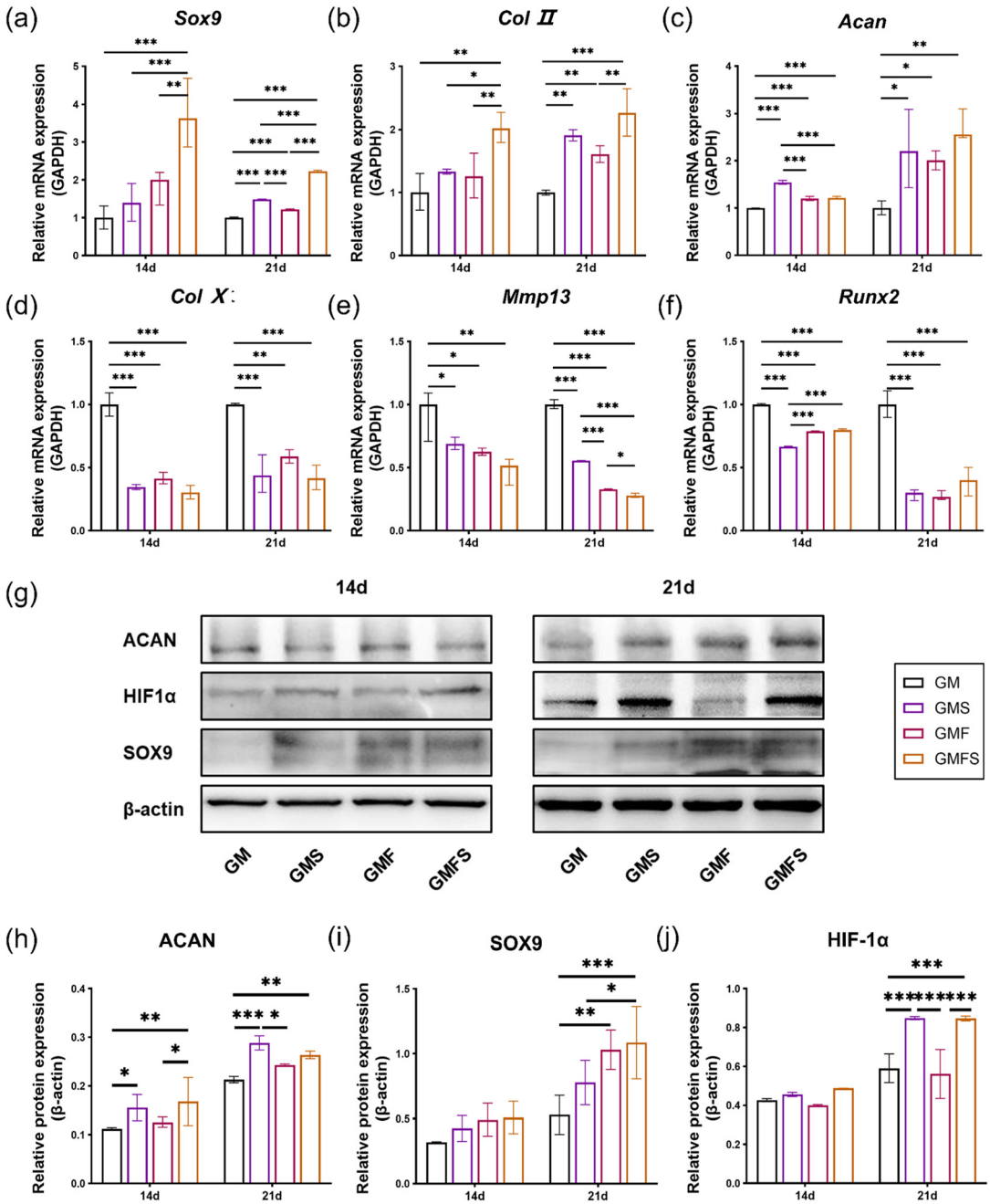

Fig. 5 *In vitro* chondrogenic effect of various hydrogels after co-culture with BMSCs for 14 and 21 days. (a–f) The relative expression of chondrogenic-related genes (*Sox9*, *Col II*, *Acan*, *Col X*, *Mmp13*, *Runx2*) in different groups *via* qPCR examination. (g–j) The expression of chondrogenic-related proteins (SOX9, ACAN and HIF-1α) in different groups *via* western blot examination (***$p < 0.001$, **$p < 0.01$, *$p < 0.05$).

The inclusion of FT also promoted *Sox9*, *Col II*, and *Acan*, but to a lesser extent than Sr^{2+}. Notably, the combined effect of Sr^{2+} and FT led to a significant increase in *Sox9* and *Col II* expression. However, after 21 days, there were no statistically significant differences between the Sr^{2+}-containing hydrogel groups regarding the increase in *Col II* and *Acan* expression or the inhibition of *Col X* and *Runx2* expression.

To evaluate the impact of each hydrogel group on the chondrogenic differentiation of BMSCs, we assessed the expression of chondrogenic-related proteins using western blotting after 14 and 21 days of co-culture with the hydrogels. The proteins analyzed included SOX9, ACAN, and HIF-1α. The results, shown in Fig. 5g–j, indicate that the addition of Sr^{2+} enhanced the levels of SOX9 and ACAN, consistent with the PCR results at day 21. While no statistically significant differences in HIF-1α expression were observed between the groups at 14 days, Sr^{2+} significantly increased HIF-1α levels at 21 days. The addition of FT did not have a significant effect on HIF-1α expression.

Articular cartilage is an avascular and aneural tissue, where chondrocytes are adapted to hypoxic or anoxic environments.[29] Hypoxia-inducible factor 1-alpha (HIF-1α) is present exclusively under hypoxic conditions and provides cytoprotection. HIF-1α translocates to the nucleus, where it interacts with hypoxia-sensitive target genes to regulate angiogenesis, energy metabolism, and apoptosis during hypoxia.[30] In OA, cartilage catabolism is associated not only with extracellular matrix (ECM) degeneration but also with chondrocyte apoptosis. The elevated rate of apoptosis in articular cartilage may significantly contribute to OA pathogenesis.[31,32] Apoptosis in OA cartilage disrupts cartilage homeostasis.[33] It has been demonstrated that hypoxic environments are crucial for promoting cartilage repair and regeneration.[34] Zhang Chi *et al.* confirmed through immunoprecipitation that HIF-1α and SOX9 interact to enhance chondrogenesis.[35] Knockdown of the HIF-1α promoter site inhibited SOX9 activation, while SOX9 expression under hypoxic conditions increased two-fold compared to normoxic conditions. Additionally, it has been reported that silicon (Si) and strontium (Sr) can stimulate cartilage formation by activating the HIF-1α signaling pathway. Deng *et al.* used 3D-printed $Sr_5(PO_4)_2SiO_4$ (SPS) bioactive ceramic scaffolds to repair cartilage and subchondral bone defects, finding that these scaffolds significantly stimulated chondrocyte proliferation and maturation while inhibiting inflammation.[36] The underlying mechanisms may involve cartilage regeneration stimulation by Sr and Si ions through synergistic activation of the HIF pathway, as well as protection of chondrocytes from joint inflammation through autophagy induction and hedgehog pathway inhibition. Cai *et al.* prepared a strontium-doped bio-glass crosslinked *in situ* injectable hydrogel, and *in vivo* experiments showed up-regulation of the HIF-1α signaling pathway in both the SA/BG and SA/SrBG groups, with the highest HIF-1α expression observed in the SA/SrBG group.[11]

3.9 Repair effect of hydrogel on cartilage defect model *in vivo*

The macroscopic results of defect repair at 8 and 12 weeks post-surgery are illustrated in Fig. 6. At 8 weeks, no hydrogel residue was observed in the surgical area of any experimental group, indicating that the hydrogel had been completely absorbed and degraded *in vivo*. Repair tissue was visible at the injury site across all groups. However, in the blank and GM groups, only fibrous tissue with a rough surface was observed. In these groups, the height of the repaired tissue was significantly lower than that of the surrounding normal cartilage, the surface was uneven, and the defect margins remained visible. Conversely, the GMS, GMF, and GMFS groups exhibited repair tissue that largely filled the defect area, though the defect

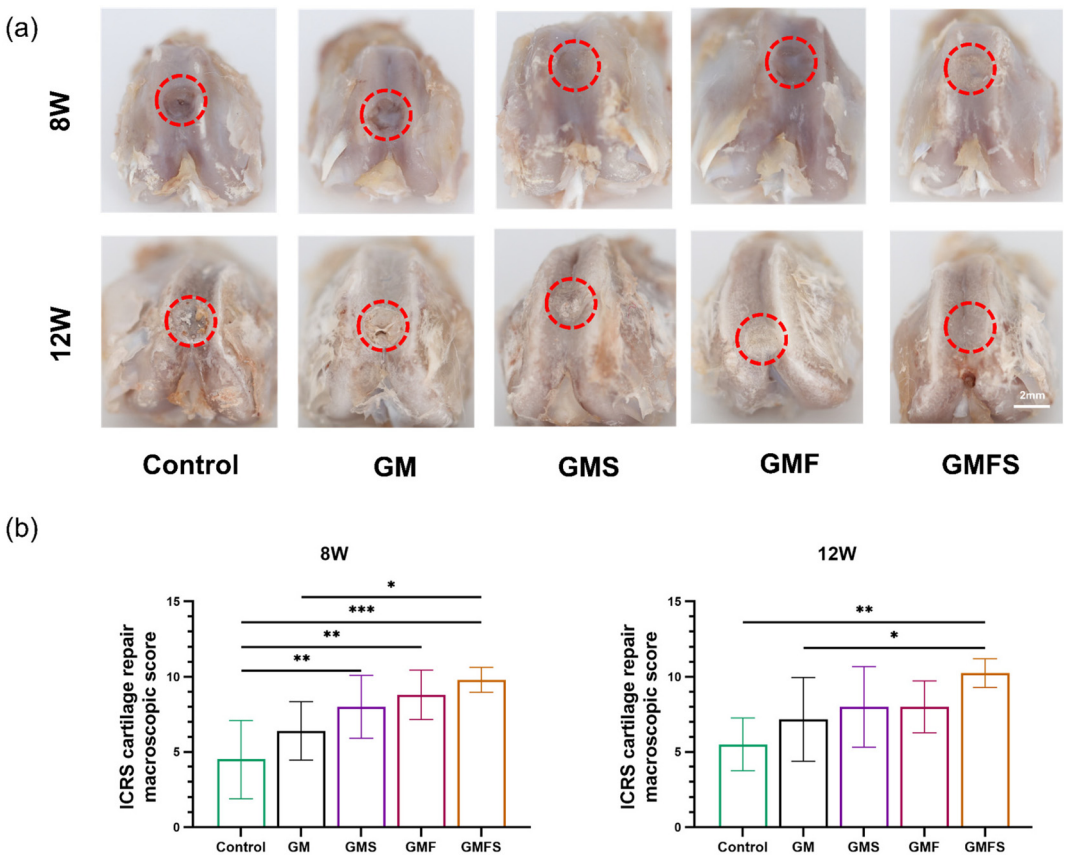

Fig. 6 Gross evaluations of repaired cartilages. (a) Macroscopic observation of repaired cartilages at 8 and 12 weeks. (b) ICRS macroscopic scores of repaired cartilages at 8 and 12 weeks (n = 6) (***p < 0.001, **p < 0.01, *p < 0.05).

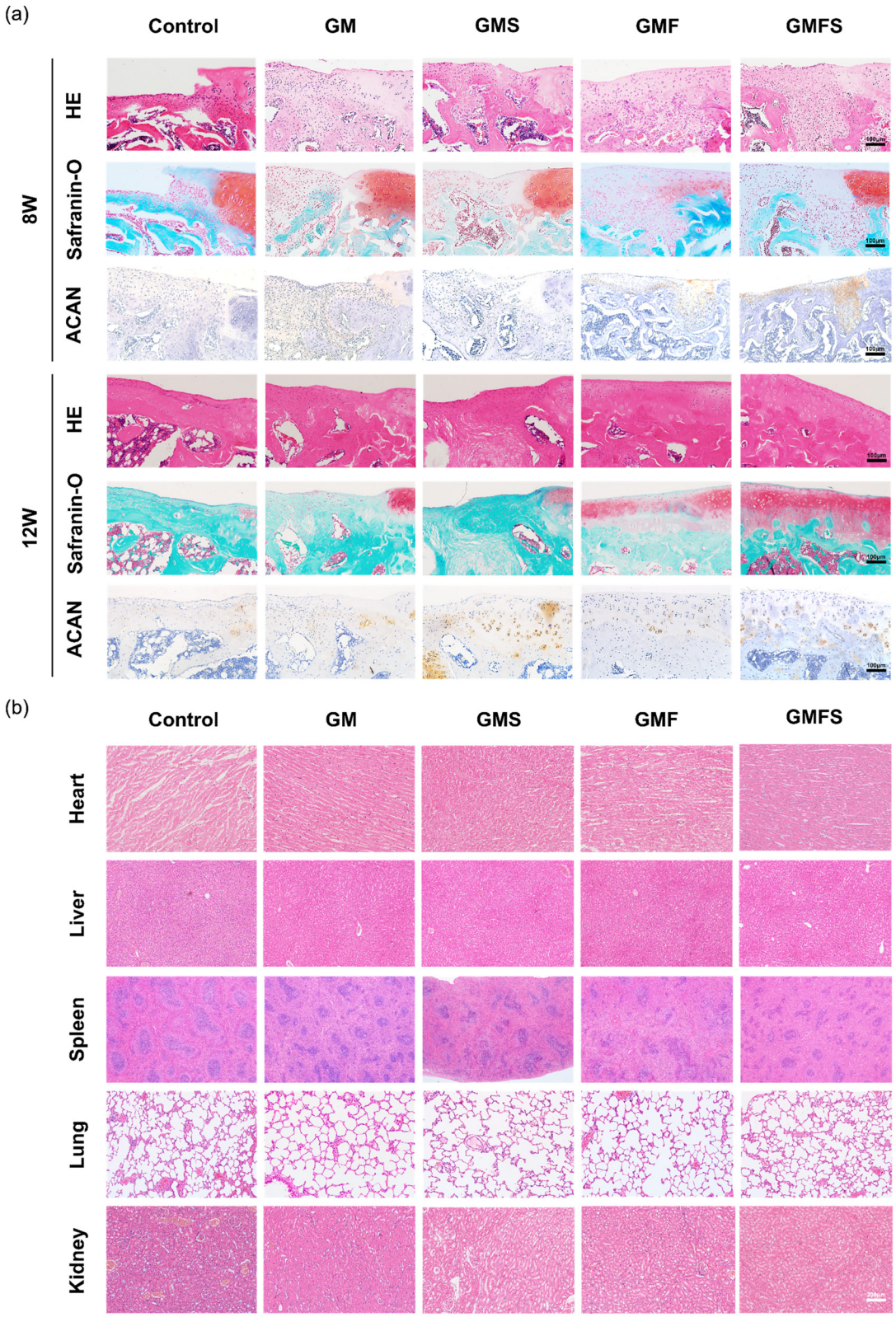

Fig. 7 (a) Histomorphological evaluations of repaired cartilages at 8 and 12 weeks: HE staining results, Safranin O-fast green staining result and ACAN immunohistochemical staining results. (b) Histomorphological evaluations of the five viscera of rats in each group at 12 weeks.

borders were still discernible. At 12 weeks, the repaired tissue in the blank group remained lower in height compared to the surrounding normal cartilage. In contrast, the hydrogel group's repaired tissue approximated the height of the surrounding normal cartilage. Fissures were present in the GM group's repaired tissue, and the defect border remained visible. The GMS and GMF groups also showed visible defect borders but lacked fissures. The GMFS group demonstrated a smooth surface with no discernible border between the repaired tissue and the surrounding normal cartilage. The ICRS macroscopic score indicated that, at both 8 and 12 weeks, the GMFS group achieved superior repair compared to the other groups.

The histomorphological staining results are presented in Fig. 7a. At 8 weeks post-surgery, all groups exhibited fibrous tissue in the repair areas. However, subsidence was noted at the defect boundary in the blank and GM groups. By 12 weeks postoperatively, fibrous tissue persisted in the blank, GM, and GMS groups, with an uneven surface. In contrast, the GMF and GMFS groups displayed cartilaginous tissues with smooth surfaces, which were seamlessly integrated with the surrounding normal cartilage. Safranin O staining, which highlights polysaccharides in cartilage, showed that the deeper red coloration indicates higher polysaccharide content. At 12 weeks, the repair tissues in the GMF and GMFS groups were red, with the GMFS group exhibiting a more intense red hue, signifying the highest polysaccharide content. Immunohistochemical staining corroborated the presence of aggrecan in the repaired tissues, aligning with the safranin O staining results. The GMFS group had the highest aggrecan content at 12 weeks postoperatively.

Hydrogel-based drug delivery systems offer several advantages, including localized drug administration, prolonged drug release, and three-dimensional physical support. These properties can help minimize joint damage by reducing physical friction in inflammatory arthritis. Strontium, positioned directly below calcium in the periodic table, shares many physical and chemical properties with calcium. In the human body, strontium is absorbed similarly to calcium, functioning as a lighter homolog of calcium. In biological systems, strontium partially replaces calcium.[37] It has been reported that strontium, as a trace element, positively influences cartilage and subchondral bone health.[12,38] Fenbo Ma *et al.* developed a strontium alginate/chondroitin sulfate (Alg/CS-Sr) hydrogel for cartilage tissue engineering.[39] Their research demonstrated that this hydrogel could inhibit apoptosis, promote cartilage defect repair in rabbits, and exert anti-inflammatory effects during the repair process. Yu *et al.* found that high-dose strontium ranelate treatment reduced cartilage degeneration and subchondral bone remodeling in rat osteoarthritis models.[24] Our preliminary studies using a rat cartilage defect repair model suggest that a strontium-loaded lubricating hydrogel can enhance the repair of joint cartilage defects.

3.10 Biosafety assessment *in vivo*

Tryptophan is an essential amino acid in the human body.[40] FT is a modified derivative of tryptophan that includes a protective group, allowing it to be metabolized slowly into various bioactive compounds *in vivo*.[41] This characteristic provides a theoretical basis for the biosafety of FT-loaded hydrogels. Epidemiological studies indicate that the concentration of strontium in drinking water may be negatively correlated with the incidence and mortality rates of various cardiovascular diseases.[42] Histological analyses of the heart, liver, spleen, lungs, and kidneys of animals were conducted to evaluate potential systemic effects of the designed system. As illustrated in Fig. 7b, HE stained sections did not reveal any significant alterations in the experimental groups after 12 weeks.

4. Conclusion

In this study, we developed strontium-loaded GelMA-FT hydrogels that exhibit lubrication properties and excellent biocompatibility, aimed at enhancing cartilage repair in a rat model of articular cartilage defects. The implantation of GMFS hydrogels resulted in significantly superior histological repair of cartilage compared to the GelMA hydrogel-only group. The findings indicate that the FT supramolecular network within the hydrogel plays a crucial role in providing lubrication in the defect area under shear stress. Furthermore, strontium—recognized as an essential trace element for the human body—effectively induces chondrogenesis in both *in vitro* and *in vivo* environments, with its sustained release positively contributing to the repair process. This dual-network hydrogel architecture effectively overcomes the limitations associated with the exclusive use of GelMA hydrogels, thereby facilitating the rehabilitation of articular cartilage defects.

Author contributions

Congcong Duan: writing – original draft, validation, methodology, data curation, conceptualization. Hongyue Jiang: writing – original draft, conceptualization, material synthesis, data curation. Shichen Zhang: software, formal analysis. Yixing Wang: animal experimentation. Peng Liu: animal experimentation. Bin Xu: writing – review & editing, conceptualization. Wenjing Tian: supervision, project administration. Bing Han: writing – review & editing, supervision, project administration, funding acquisition, conceptualization.

Data availability

All data from this project are available from the corresponding author upon reasonable request.

Conflicts of interest

The authors declare that they have no known competing financial interests or personal relationships that could have appeared to influence the work reported in this paper.

Acknowledgements

This work was supported by Science and Technology Development Program Project of Jilin province (232668GH0104111076 and 222604YY010498391).

References

1 J. Farr and J. Q. Yao, Chondral Defect Repair with Particulated Juvenile Cartilage Allograft, *Cartilage*, 2011, **2**(4), 346–353.
2 W. Lin and J. Klein, Recent Progress in Cartilage Lubrication, *Adv. Mater.*, 2021, **33**(18), 2005513.
3 R. F. Loeser, S. R. Goldring, C. R. Scanzello, *et al.*, Osteoarthritis: A disease of the joint as an organ, *Arthritis Rheum.*, 2012, **64**(6), 1697–1707.
4 D. Gan, Z. Wang, C. Xie, *et al.*, Mussel–Inspired Tough Hydrogel with In Situ Nanohydroxyapatite Mineralization for Osteochondral Defect Repair, *Adv. Healthcare Mater.*, 2019, **8**(22), 1901103.
5 X. Ai, Y. Duan, Q. Zhang, *et al.*, Cartilage–targeting ultrasmall lipid–polymer hybrid nanoparticles for the prevention of cartilage degradation, *Bioeng. Transl. Med.*, 2020, **6**(1), e10187.
6 Y. Cho, S. Jeong, H. Kim, *et al.*, Disease-modifying therapeutic strategies in osteoarthritis: current status and future directions, *Exp. Mol. Med.*, 2021, **53**(11), 1689–1696.
7 H. Kwon, W. E. Brown, C. A. Lee, *et al.*, Surgical and tissue engineering strategies for articular cartilage and meniscus repair, *Nat. Rev. Rheumatol.*, 2019, **15**(9), 550–570.
8 L. Han, K. Liu, M. Wang, *et al.*, Mussel-Inspired Adhesive and Conductive Hydrogel with Long-Lasting Moisture and Extreme Temperature Tolerance, *Adv. Funct. Mater.*, 2018, (3), 28.
9 X. Zhang, J. Wang, H. Jin, *et al.*, Bioinspired Supramolecular Lubricating Hydrogel Induced by Shear Force, *J. Am. Chem. Soc.*, 2018, **140**(9), 3186–3189.
10 Y. Bai, S. He, Y. Lian, *et al.*, Self-Lubricating Supramolecular Hydrogel for In-Depth Profile Control in Fractured Reservoirs, *ACS Omega*, 2020, **5**(13), 7244–7253.
11 Z. Cai, Y. Li, W. Song, *et al.*, Anti-Inflammatory and Prochondrogenic In Situ-Formed Injectable Hydrogel Crosslinked by Strontium-Doped Bioglass for Cartilage Regeneration, *ACS Appl. Mater. Interfaces*, 2021, **13**(50), 59772–59786.
12 V. Zaichick, Chemical Elements of Human Bone Tissue Investigated by Nuclear Analytical and Related Methods, *Biol. Trace Elem. Res.*, 2013, **153**(1–3), 84–99.
13 E. Storey, Intermittent bone changes and multiple cartilage defects in chronic strontium rickets in rats, *J. Bone Joint Surg. Br.*, 1962, **44**(1), 194–208.
14 R. Robison, K. A. Law and A. H. Rosenheim, Deposition of strontium salts in hypertrophic cartilage in vitro, *Biochem. J.*, 1936, **30**(1), 66–68.
15 N. Okita, Y. Honda, N. Kishimoto, *et al.*, Supplementation of Strontium to a Chondrogenic Medium Promotes Chondrogenic Differentiation of Human Dedifferentiated Fat Cells, *Tissue Eng., Part A*, 2015, **21**(9–10), 1695–1704.
16 Y. Hao, Y. Xiang-Wen, H. Jia-Jing, *et al.*, Effect of strontium ranelate on chondrogenic differentiation of rat bone mesenchymal stem cells, *Shanghai J. Stomatol.*, 2022, **31**(1), 24.
17 D. B. A. I. Van, B. Bogdanov and N. De Rooze, *Et Al.*Structural and rheological properties of methacrylamide modified gelatin hydrogels, *Biomacromolecules*, 2000, **1**(1), 31–38.
18 I. Pepelanova, K. Kruppa, T. Scheper, *et al.*, Gelatin-Methacryloyl (GelMA) Hydrogels with Defined Degree of Functionalization as a Versatile Toolkit for 3D Cell Culture and Extrusion Bioprinting, *Bioengineering*, 2018, **5**(3), 55.
19 M. Bartnikowski, N. J. Bartnikowski, M. A. Woodruff, *et al.*, Protective effects of reactive functional groups on chondrocytes in photocrosslinkable hydrogel systems, *Acta Biomater.*, 2015, **27**, 66–76.
20 Y. S. Zhang, Khademhosseini A. Advances in engineering hydrogels, *Science*, 2017, **356**(6337), eaaf3627.
21 Y. Li, L. Xiao, D. Wei, *et al.*, Injectable Biomimetic Hydrogel Guided Functional Bone Regeneration by Adapting Material Degradation to Tissue Healing, *Adv. Funct. Mater.*, 2023, **33**(19), 2213047.
22 D. Gan, T. Xu, W. Xing, *et al.*, Mussel-inspired dopamine oligomer intercalated tough and resilient gelatin methacryloyl (GelMA) hydrogels for cartilage regeneration, *J. Mater. Chem. B*, 2019, **7**(10), 1716–1725.
23 Y. Han, J. Yang, W. Zhao, *et al.*, Biomimetic injectable hydrogel microspheres with enhanced lubrication and controllable drug release for the treatment of osteoarthritis, *Bioact. Mater.*, 2021, **6**(10), 3596–3607.
24 D.-G. Yu, H.-F. Ding, Y.-Q. Mao, *et al.*, Strontium ranelate reduces cartilage degeneration and subchondral bone remodeling in rat osteoarthritis model, *Acta Pharmacol. Sin.*, 2013, **34**(3), 393–402.
25 X. Cui, C. Huang, M. Zhang, *et al.*, Enhanced osteointegration of poly(methylmethacrylate) bone cements by incorporating strontium-containing borate bioactive glass, *J. R. Soc., Interface*, 2017, **14**(131), 20161057.
26 H. Cheng, W. Xiong, Z. Fang, *et al.*, Strontium (Sr) and silver (Ag) loaded nanotubular structures with combined osteoinductive and antimicrobial activities, *Acta Biomater.*, 2016, **31**, 388–400.
27 C. Zhou, A.-T. Xu, D.-D. Wang, *et al.*, The effects of Sr-incorporated micro/nano rough titanium surface on rBMSC migration and osteogenic differentiation for rapid osteointegration, *Biomater. Sci.*, 2018, **6**(7), 1946–1961.
28 M. Huang, R. G. Hill and S. C. F. Rawlinson, Strontium (Sr) elicits odontogenic differentiation of human dental pulp stem cells (hDPSCs): A therapeutic role for Sr in dentine repair?, *Acta Biomater.*, 2016, **38**, 201–211.
29 J. Zhang, Y. Hu, Z. Wang, *et al.*, Hypoxia-inducible factor expression is related to apoptosis and cartilage degradation in temporomandibular joint osteoarthritis, *BMC Musculoskeletal Disord.*, 2022, **23**(1), 583.

30 G. N. Masoud and W. Li, HIF-1α pathway: role, regulation and intervention for cancer therapy, *Acta Pharm. Sin. B*, 2015, **5**(5), 378–389.
31 G. A. Conlon and G. I. Murray, Recent advances in understanding the roles of matrix metalloproteinases in tumour invasion and metastasis, *J. Pathol.*, 2019, **247**(5), 629–640.
32 H. Hwang and H. Kim, Chondrocyte Apoptosis in the Pathogenesis of Osteoarthritis, *Int. J. Mol. Sci.*, 2015, **16**(11), 26035–26054.
33 X. Houard, M. B. Goldring and F. Berenbaum, Homeostatic Mechanisms in Articular Cartilage and Role of Inflammation in Osteoarthritis, *Curr. Rheumatol. Rep.*, 2013, **15**(11), 375.
34 N. Zhou, N. Hu, J.-Y. Liao, *et al.*, HIF-1α as a Regulator of BMP2-Induced Chondrogenic Differentiation, Osteogenic Differentiation, and Endochondral Ossification in Stem Cells, *Cell. Physiol. Biochem.*, 2015, **36**(1), 44–60.
35 C. Zhang, F. Yang, R. Cornelia, *et al.*, Hypoxia-inducible factor-1 is a positive regulator of Sox9 activity in femoral head osteonecrosis, *Bone*, 2011, **48**(3), 507–513.
36 C. Deng, H. Zhu, J. Li, *et al.*, Bioactive Scaffolds for Regeneration of Cartilage and Subchondral Bone Interface, *Theranostics*, 2018, **8**(7), 1940–1955.
37 S. Pors Nielsen, The biological role of strontium, *Bone*, 2004, **35**(3), 583–588.
38 W. E. Cabrera, I. Schrooten, M. E. De Broe, *et al.*, Strontium and Bone, *J. Bone Miner. Res.*, 1999, **14**(5), 661–668.
39 F. Ma, Y. Ge, N. Liu, *et al.*, In situ fabrication of a composite hydrogel with tunable mechanical properties for cartilage tissue engineering, *J. Mater. Chem. B*, 2019, **7**(15), 2463–2473.
40 C. Xue, G. Li, Q. Zheng, *et al.*, Tryptophan metabolism in health and disease, *Cell Metab.*, 2023, **35**(8), 1304–1326.
41 K. Tao, A. Levin, L. Adler-Abramovich, *et al.*, Fmoc-modified amino acids and short peptides: simple bio-inspired building blocks for the fabrication of functional materials, *Chem. Soc. Rev.*, 2016, **45**(14), 3935–3953.
42 E. B. Dawson, M. J. Frey, T. D. Moore, *et al.*, Relationship of metal metabolism to vascular disease mortality rates in Texas, *Am. J. Clin. Nutr.*, 1978, **31**(7), 1188–1197.